scientific reports

Check for updates

OPEN

Defective membrane repair machinery impairs survival of invasive cancer cells

F. Bouvet[1], M. Ros[2], E. Bonedeau[1], C. Croissant[1], L. Frelin[1], F. Saltel[2], V. Moreau[2] & A. Bouter[1]✉

Cancer cells are able to reach distant tissues by migration and invasion processes. Enhanced ability to cope with physical stresses leading to cell membrane damages may offer to cancer cells high survival rate during metastasis. Consequently, down-regulation of the membrane repair machinery may lead to metastasis inhibition. We show that migration of MDA-MB-231 cells on collagen I fibrils induces disruptions of plasma membrane and pullout of membrane fragments in the wake of cells. These cells are able to reseal membrane damages thanks to annexins (Anx) that are highly expressed in invasive cancer cells. In vitro membrane repair assays reveal that MDA-MB-231 cells respond heterogeneously to membrane injury and some of them possess a very efficient repair machinery. Finally, we show that silencing of AnxA5 and AnxA6 leads to the death of migrating MDA-MB-231 cells due to major defect of the membrane repair machinery. Disturbance of the membrane repair process may therefore provide a new avenue for inhibiting cancer metastasis.

Abbreviations

Anx	Annexins
AnxA1	Annexin-A1
AnxA2	Annexin-A2
AnxA5	Annexin-A5
AnxA6	Annexin-A6
Ca^{2+}	Calcium
DPBS	Dulbecco's phosphate buffer saline
MOI	Multiplicity of infection
PS	Phosphatidylserine

In cells exposed to mechanical stress, such as skeletal or cardiac muscle cells, epithelial cells and endothelial cells, plasma membrane disruption is a physiological event that occurs frequently[1–4]. These cells possess a molecular machinery enabling repair of membrane disruptions at the minute scale[5,6]. The absence of membrane resealing leads to cell death and may contribute to the development of degenerative diseases, such as muscular dystrophies[7,8]. Various mechanisms enabling membrane repair have been described such as protein clogging, membrane injury endocytosis or shedding, and lipid patching[6]. Influx of Ca^{2+} from extracellular (mM-) to intracellular (µM-range concentration) is the main trigger of membrane repair, which relies mainly on Ca^{2+}-sensitive membrane binding proteins such as dysferlin[9], AHNAK[10], calpains[11] and Anx[12–16]. MG53 is also a crucial component of the membrane repair machinery, yet it is activated by the change of oxidation state instead of Ca^{2+} increase due to entry of extracellular milieu[17]. In the case of mechanical tear, the membrane repair machinery drives the fusion of intracellular vesicles, which builds a lipid "patch". This lipid "patch" is recruited to the wounded site via an exocytic-like process for resealing the damaged plasma membrane[18–20].

Anx appear to be crucial components of the membrane repair machinery in a wide range of cell types. The Anx family consists of twelve soluble proteins in mammals, named AnxA1 to A13 (the number 12 is non-assigned)[21]. In a Ca^{2+}-dependent manner, Anx share the property of binding to membranes exposing negatively charged phospholipids[21,22]. They exhibit little specificity for anionic lipid head-groups and variable threshold-value of Ca^{2+} concentration for membrane binding[23–25]. In mouse primary muscle cells, AnxA1 and AnxA2 may be responsible for fusion of intracellular vesicles and recruitment of lipid "patch" to the membrane disruption

[1]Institute of Chemistry and Biology of Membranes and Nano-Objects, UMR 5248, CNRS, University of Bordeaux, IPB, Bât. B14, Allée Geoffroy Saint Hilaire, 33600 Pessac, France. [2]INSERM, BaRITOn, U1053, University of Bordeaux, 33000 Bordeaux, France. ✉email: a.bouter@cbmn.u-bordeaux.fr

site by interacting with dysferlin[12]. In skeletal muscle of zebrafish, it has been proposed that membrane repair is based on the establishment of a highly ordered scaffold involving dysferlin, AnxA6, AnxA2 and AnxA1[14]. In the presence of Ca^{2+}, AnxA5 presents the property of rapidly assembling into trimers and self-organizing into 2D ordered arrays, when it binds to biological membranes[26–29]. We have shown that AnxA5 promotes membrane repair by forming 2D arrays at the torn membrane edges, thus strengthening the membrane, preventing the expansion of wound and facilitating the final steps of membrane resealing[13,20,30].

As a defect in membrane repair is responsible for the development of muscular dystrophies[8,31,32], major attention has focused on membrane repair of skeletal muscle cells, leaving membrane repair in other tissues and in other pathologies almost not characterized. Cancer cell metastasis is a cascade of events that allows the dissemination of the disease from the site of origin into peripheral vessels, and, subsequently, other organs. One of the hallmarks of metastatic cells is their ability to invade the surrounding tissues. Tumor cell migration and invasion require actin cytoskeleton remodeling, which increases membrane dynamics and reduces stiffness of the plasma membrane[33]. In addition, invasive cancer cells are submitted to tremendous shearing forces, due to their migration through the extracellular milieu and their invasion of distant tissue, which may lead to numerous plasma membrane damages (see for review[34]).

Even though few studies have linked membrane repair and cancer, numerous works have highlighted incidentally a positive correlation between major actors of the membrane repair machinery and tumor invasion. For instance, it has been observed that the overexpression of many Anx enhances tumor aggressiveness and is a factor of poor prognosis in various cancers such as breast cancer[35–42]. In addition, Anx inhibition significantly reduces proliferation, migration and invasion abilities of tumor cells, without knowing accurate mechanism[43–47]. Credit has to be given to J. Jaiswal and J. Nylandsted for the first investigations describing membrane repair machinery in cancer cells. They show that the AnxA2/S100A11 complex promotes membrane repair by remodeling actin cytoskeleton and facilitating excision of the damaged membrane area in MCF-7 cells[48]. Since then, AnxA4 and AnxA6 have also been shown to participate in membrane repair of MCF-7 cells by inducing respectively membrane curvature from the edges of the torn membrane and constriction force to pull the wound edges together[15]. Finally, the excision of damaged membrane by ESCRT-mediated shedding requires AnxA7 in MCF-7 cells[49]. Altogether, these findings suggest that an efficient membrane repair machinery composed by Anx exists in cancer cells and may facilitate tumor invasion processes.

The aim of the present study was to investigate whether silencing of proteins from the membrane repair machinery may impair survival of cancer cells during the migration process. To address this question, we have analyzed the behavior of MDA-MB-231 cells seeded on glass coverslip coated with type I collagen (collagen I) fibrils. MDA-MB-231 breast tumor cell line exhibits strong capacity of invasiveness in vitro and in vivo as well[50]. This cell line has constituted therefore a suitable model for analyzing the effect of invasiveness on cell membrane disruption and repair. Collagen I is the most abundant extracellular matrix protein in vertebrates and is overexpressed in a large number of cancers[51,52]. The effect of collagen I on tumor cells is complex and paradoxical. Initially expected to form a physical barrier for limiting the progression of the tumor, collagen I has proved to be a powerful inducer of linear invadosomes, which in turn activate cell invasion by promoting matrix metalloproteases activity that degrades extracellular matrix[53]. After having characterized that AnxA5 and AnxA6 belong to the membrane repair machinery of MDA-MB-231 cells, we compared the responses to collagen I-mediated membrane injury of control cells to cells rendered deficient for AnxA5 and/or AnxA6. Our results lead us to propose that membrane repair machinery may be considered as a promising target for weakening cancer cell invasion.

Materials and methods

Cell culture media and reagents were from ThermoFisher Scientific (Waltham, MA, USA) except when otherwise stated.

Cell culture. MDA-MB-231 cells were cultured in Dulbecco modified Eagle's minimal essential medium (DMEM) containing 4 mM Glutamax and supplemented with 10% fetal bovine serum and penicillin/streptomycin (100 U/mL and 100 µg/mL). The choriocarcinoma BeWo cell line was cultured in Ham's F12K medium containing 5 mM L-glutamine and supplemented with 20% fetal bovine serum and penicillin/streptomycin (100 U/mL and 100 µg/mL). Both cell types were maintained at 37 °C in a 5% CO_2 humidified incubator.

Coating. All experiments were performed in 35-mm glass bottom dishes equipped with a square patterned coverslip (MatTek, Ashland, USA). Coating was performed as previously described[54]. Briefly, the glass coverslip was first coated for 20 min at RT with 1 mg/mL gelatin, which was fixed by 0.5% glutaraldehyde for 40 min at RT. After three washes with Dulbecco's phosphate buffer saline (DPBS) containing 0.9 mM $CaCl_2$ (DPBS + Ca^{2+}), collagen I at 0.5 mg/mL was incubated for 4 h at 37 °C. After removing the excess of collagen I, $4{\cdot}10^4$ cells in growth medium were subsequently seeded and cultured for 24 h.

Kinetics study of MDA-MB-231 migration by phase contrast video-microscopy. Phase-contrast video-microscopy was performed using the Leica DMI6000B microscope equipped with CCD camera (6.45 µm pixel dimension, 1392 × 1040 pixels, Leica) 48 h after cell seeding. Dishes were positioned in the tempered (37 °C) humidified chamber at least 30 min before beginning kinetics study. Unless otherwise indicated, kinetics studies lasted 2 h using an acquisition interval of 1 min. Tracking of cells was performed using the MTrackJ plugin from ImageJ software[55]. For each condition, at least 100 cells from three independent experiments were analyzed.

Kinetics study of Fluo4AM-loaded MDA-MB-231 migration by fluorescence microscopy. Working solution was prepared by dissolving 50 µg of Fluo-4AM in DMSO at a final concentration of 1 mM. 10 µL of Fluo-4AM working solution were mixed with 8 µL of Pluronic F-127 (Sigma). The mixture was vortexed and diluted in 2 mL growth medium, which were added on cells for 1 h at 37 °C. After one wash with DPBS + Ca^{2+}, cells were incubated in growth medium. Fluorescence and phase-contrast video-microscopy was performed using the Leica DMI6000B microscope. Kinetics studies lasted 2 h with 30-s interval acquisitions.

CellMask Orange staining. A fresh working solution was prepared by diluting the commercial CellMask Orange stock solution at 1:1000 in 2 mL DPBS + Ca^{2+}. After 2 h of migration on collagen I, the growth medium of MDA-MB-231 cells was replaced by the CellMask Orange working solution for 5 min incubation at 37 °C. Cells were washed three times in DPBS + Ca^{2+}solution and then fixed in 4% PFA for 10 min at RT. After three washes in DPBS + Ca^{2+}, CellMask Orange staining was observed using the cube U-MWG2 containing in a band-pass excitation filter (510–550 nm), a dichroic mirror (50% transmission from 570 nm) and a long-pass emission filter (threshold 590 nm) from the conventional fluorescence IX81 microscope (Olympus). Images were analyzed with the ImageJ software.

Membrane rupture and repair assay. Membrane repair assay differed slightly from our previous studies[56]. MDA-MB-231 cells were cultured in complete growth medium on 18*18 mm glass coverslips (Nunc). A solution of 5 µg/mL FM1-43 (ThermoFisher Scientific, Waltham, MA, USA) in D-PBS containing 2 mM Ca^{2+} was maintained over ice and subsequently added in a homemade coverslip cell chamber (Supplementary Fig. 1), where cells containing coverslip was mounted. To induce membrane damage, cells were irradiated at 820 nm with a tunable pulsed depletion laser Mai Tai HP (Spectra-Physics, Irvine, USA) of an upright two-photon confocal scanning microscope (TCS SP5, Leica) equipped with an HCX PL APO CS 63.0 × 1.40 oil-objective lens. Irradiation consisted of 1 scan (1.3 s) of a 1 µm × 1 µm area with a power of 110 (± 5) mW. 512 × 512 images were acquired at 1.3 s intervals with pinhole set to 1 Airy unit. Membrane rupture and repair processes were monitored by measuring variations in fluorescence intensity of FM1-43 as previously described[56]. FM1-43 was excited by the 488-nm laser line (intensity set at 30% of maximal power) and fluorescence emission was measured between 520 and 650 nm. For quantitative analysis, the fluorescence intensity was integrated over the whole cell surface and corrected for the fluorescence value recorded before irradiation, using ImageJ software.

Western-blot. $2{\cdot}10^6$ cells were trypsinized, pelleted and re-suspended in 300 µL of D-PBS supplemented with 1 mM EGTA. Protein extracts were obtained by sonicating ice-cold cell suspension with a Branson digital sonifier (amplitude 20%, duration 2 min, interval 5 s and pulse 5 s). Two successive centrifugations at 13,000 g for 1 min allowed to remove cell debris. 10 µg protein extracts were separated on a 10% SDS-PAGE for detection of Anx. Semi-dry electrophoretic transfer (Bio-Rad, Hercules, CA, USA) onto PVDF membrane was performed for 1 h at 100 V. The cellular content in AnxA1 (37 kDa), AnxA2 (36 kDa), AnxA4 (32 kDa), AnxA5 (35 kDa), AnxA6 (68 kDa), and glyceraldehyde-3-phosphate deshydrogenase (GAPDH, loading control, 37 kDa) was detected with rabbit anti-AnxA1 polyclonal antibody (PA1006, BosterBio, Pleasanton, CA, USA), mouse anti-AnxA2 monoclonal antibody (3E8-B6, Sigma, Saint-Louis, MO, USA), mouse anti-AnxA4 monoclonal antibody (SAB4200121, Sigma), mouse anti-AnxA5 monoclonal antibody (AN5, Sigma), mouse anti-AnxA6 monoclonal antibody (sc-271859, Santa cruz Biotechnology), and rabbit anti-GAPDH polyclonal antibody (FL-335, Santa Cruz Biotechnology), respectively. All primary antibodies were diluted 1:1000 in saturation solution composed by Tris buffer saline (10 mM Tris, 150 mM NaCl, pH 8.0) supplemented with 0.1% Tween20 and 5% non-fat dry milk. Revelation was performed using secondary antibodies conjugated to horse-radish peroxidase (GE-Healthcare) diluted 1:2000 in saturation solution and Opti-4CN colorimetric kit (Bio-Rad). ImageJ software was used to measure the relative intensity of protein bands.

Transduction of AnxA5-targeting and/or AnxA6-targeting shRNA lentiviral particles in MDA-MB-231 cells. The following shRNA sequences, cloned into the pLKO.1 puro-vector (MISSION shRNA plasmids, Sigma), were used: AnxA5-targeting shRNA A5shRNA-1 (ref. number: TRCN0000029392): 5′-CCGGCGCGACTTCTGGAATTTACTCGAGTAAATTGCCAGA AGTCTCGCGTTTTT-3′; A5shRNA-2 (ref. number: TRCN0000029389): 5′-CCGGGCCATCAAACAAGTTATGAACTCGAGTTCATAAACTTG TTTGATGGCTTTTT-3′; AnxA6-targeting shRNA A6shRNA-1 (ref. number: TRCN0000011461): 5′-CCG GCGGGCACTTCTGCCAAGAAATCTCGAGATTTCTTGGAGAAGTGCCCGTTTTT-3′; A6shRNA-2 (ref. number: TRCN0000008686): 5′-CCGGCGGTTGGTGTTCGATGA GTATCTCGAGATACTCATCGAACA CCAACCGTTTTT-3′; scrambled shRNA (SCshRNA): 5′-CCTAAGGTTAAGTCGCCCTCGCTCGAGCGA GGGCGACTTAACCT TAGG-3′. A strong decrease (about 90%) of Anx expression has always been observed and similar results were obtained whatever the AnxshRNA used, regarding membrane repair properties after laser ablation or during migration on collagen I. For the sake of clarity, only experiments performed with A5shRNA-1 and A6shRNA-1 are presented in this manuscript.

Lentiviral-based particles containing shRNAs were produced by Bordeaux University Lentiviral Vectorology Platform (US005, Bordeaux, France) by transient transfection of 293 T cells. $2{\cdot}10^5$ MDA-MB-231 cells were cultured in a 30 mm Petri Dish for 24 h and transduction was carried out by adding concentrated lentiviral particles to the cells at multiplicity of infection (MOI) of 10 in 2 mL Opti-MEM for 24 h. Transduced cells were cultured for 24 h in growth medium and then selected in selection medium composed by 2 µg/mL puromycin in DMEM for 48 h. Cells were passaged and subsequently cultured in 25 cm^2 cell culture flask in selection medium. At each passage, a fraction of cells was used for preparing protein extracts for western-blot analysis of the expression of endogenous Anx. Co-transduction of lentiviral-based particles containing AnxA5- and AnxA6-targeting

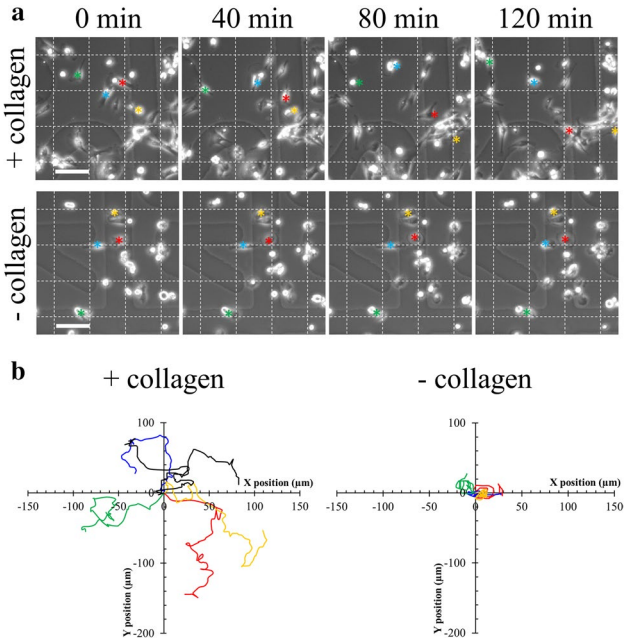

Figure 1. Effect of collagen I fibrils on the migration of MDA-MB-231 cells. (**a**) Kinetics studies by phase-contrast video-microscopy of MDA-MB-231 cells seeded on a glass coverslip coated (top panel) or not (bottom panel) with collagen I. Asterisks (red, blue, green, yellow) correspond to the position of cells of interest in the course of time. Scale bar: 100 µm. (**b**) Tracking analysis of cells presented in (**a**) was performed using MTrackJ plugin from ImageJ software. Relative position of cells migrating during two hours on glass coverslip coated (left panel) or not (right panel) with collagen I was plotted. For the sake of clarity, only four and six tracks were presented in the absence or presence of collagen, respectively. Color tracks correspond to cells marked with asterisk in (**a**).

shRNAs was performed by mixing each type of particles at MOI of 10 with $2{\cdot}10^5$ MDA-MB-231 cells, which corresponds to a final MOI of 20.

Localization of endogenous Anx in intact and damaged cells by immunofluorescence. For subcellular localization of endogenous Anx in damaged MDA-MB-231 cells, cell membrane rupture was performed according to the protocol described above, but in the absence of FM1-43 to avoid fluorescence cross-talk. After laser irradiations, cells were fixed in 1% glutaraldehyde and permeabilized in 0.1% TritonX100 diluted in DPBS + Ca^{2+}. All subsequent steps (saturation, antibody incubation and washes) were performed using 2% BSA in DPBS + Ca^{2+} solution. Primary antibodies (1:100, except for anti-AnxA5 1:400), which were the same as used for western-blot, and secondary Alexa Fluor 488-coupled anti-mouse or anti-rabbit IgG goat antibodies (1:1000, ThermoFisher Scientific) were successively incubated with cells for 1 h at 37 °C. Finally, cells were washed in DPBS + Ca^{2+} and nuclear counterstaining was performed with DAPI (Sigma). For each condition, about 30 cells from three independent experiments were analyzed.

For the subcellular localization of endogenous Anx in intact MDA-MB-231 cells, cells were cultured in 8-well Lab-Tek chambered coverglasses. Cells were immunostained according to the protocol described above for the localization of Anx in damaged cells, from the step of glutaraldehyde fixation.

Results

Collagen I fibrils favor migration of MDA-MB-231 cells and formation of migrasome. First, the migration of MDA-MB-231 cells plated on glass coverslip coated or not with collagen I was compared through analysis by phase-contrast video-microscopy (Fig. 1).

The fibrillar collagen substrate obtained in our experimental conditions has been previously characterized in depth[53,57]. Treatment with glutaraldehyde enables collagen I cross-linking, which increases the capacity of tumor cells to form invasive structures[58]. Tracking of cells was performed in both conditions by means of the MtrackJ plugin from the ImageJ software[55] and start–end distances were measured. Start–end distance is the Euclidian distance between positions of cell at t_0 and t_{end}. It therefore positively correlates with the motility of the cell. In the presence of collagen I, cells exhibited elongated shape and migrated lengthwise (Fig. 1 and Supplementary video 1), whereas in the absence, they presented mostly rounded shape and spinning movements (Fig. 1 and Supplementary video 2). Mean start–end distance of cells seeded on collagen I was significantly (P value = 5.5E−11 for Student t test) higher (103 ± 33 µm) than in the absence of collagen I (13 ± 12 µm) after 2 h of migration. We have therefore concluded that collagen I fibrils favor the migration of MDA-MB-231 cells.

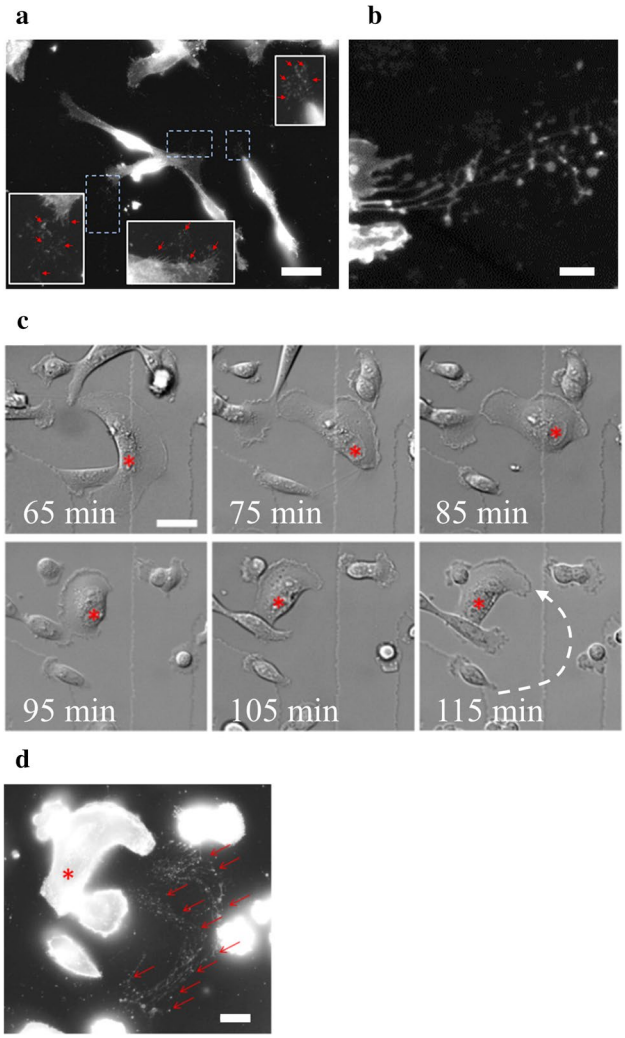

Figure 2. Presence of membrane fragments during MDA-MB-231 cell migration on collagen I fibrils. (**a**) MDA-MB-231 cells were seeded on a glass coverslip coated with collagen I. 24 h after seeding, kinetics study of cell migration was performed during 2 h by phase-contrast video-microscopy. Cells were then incubated with CellMask Orange (white). Red arrows indicate membrane material at the periphery of cells. Scale bar: 60 µm. (**b**) Observation at higher-magnification by fluorescence microscopy revealed the presence of membrane material stained by CellMask Orange (white), which appears as membrane-bound vesicular structures. Scale bar: 5 µm. (**c**) Kinetics study enabled to identify a migrating cell, for which the nucleus has been marked by a red asterisk. The dashed white arrow indicates the path of the cell during the migration. Scale bars: 40 µm. (**d**) After migration, cells were immediately incubated with CellMask Orange (white) for 5 min and fixed with 4% paraformaldehyde. Red asterisk marks the nucleus of the cell of interest presented in **c** and red arrows indicate membrane fragments present in the wake of the cell. Scale bar: 20 µm.

In order to characterize the migrasome[59,60] of MDA-MB-231 cells moving on collagen I fibrils, cells were cultured on glass coverslip coated with collagen I for 24 h. Their migration was analyzed for 2 h by phase-contrast video-microscopy and at the end of the kinetics study cells were fixed and incubated with CellMask Orange. CellMask stains are lipophilic dyes that become fluorescent upon inserting into plasma membrane. The use of glass bottom dishes equipped with a square-patterned coverslip displaying an alphanumerical code in each square enabled cell tracking during different stages of the experiment and correlation of cell migration observed by phase-contrast video-microscopy and CellMask Orange staining analyzed by fluorescence microscopy. By means of fluorescence microscopy, we systematically observed (over 7 independent experiments) the presence of cell membrane fragments in the near periphery of approximately 70% of cells (Fig. 2a). At higher magnification, cell membrane fragments appeared as membrane-bound vesicular structures (MbVS, Fig. 2b), as previously described by Yu and collaborators[59]. By analyzing the immediate surrounding of a migrating cell followed by video-microscopy (Fig. 2c and Supplementary video 3), we observed the presence of MbVS in the wake of the cell by fluorescence microscopy (Fig. 2d). We have concluded that MDA-MB-231 cells migrating on collagen I fibrils release MbVS in their wake. Formation and release of these cell structures may be induced by shearing forces existing between the extracellular collagen I fibrils and cell membrane.

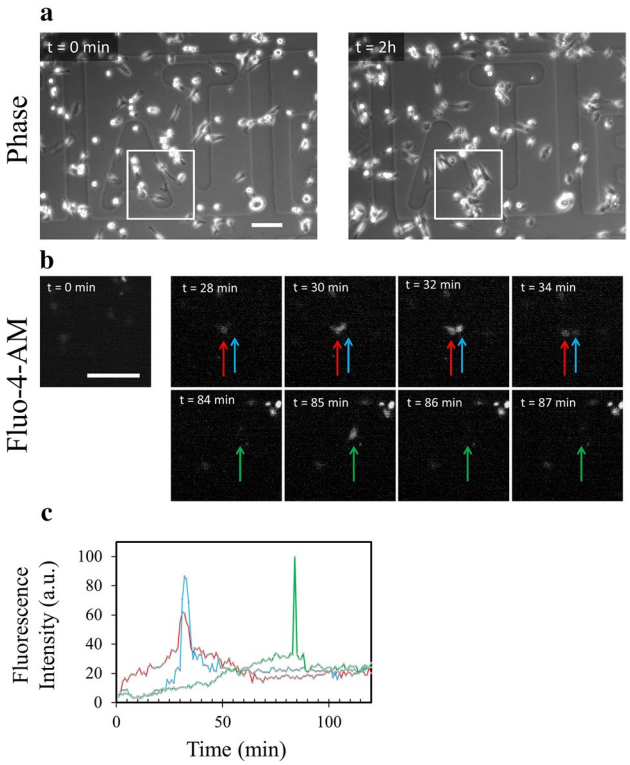

Figure 3. Highlighting membrane ruptures in migrating MDA-MB-231 cells. MDA-MB-231 cells were seeded on a glass coverslip coated with collagen I for 24 h, then incubated for 1 h at 37 °C with 2.5 µM Fluo-4-AM (white) and finally kinetics study using fluorescence microscopy was performed for 2 h. (**a**) Images in phase-contrast microscopy were acquired before and after the kinetics study. (**b**) Fluorescence intensity variations of intracellular Fluo-4-AM studied in the course of time. Each colored arrow points out a cell of interest exhibiting a strong variation of the fluorescence intensity. A strong increase of fluorescence intensity is particularly observed at t = 32 min (blue and red arrows) and t = 85 min (green arrow). A recovery of fluorescence intensity to a basal level is observed at t = 34 min (blue and red arrows) and t = 86 min (green arrow). Scale bar: 100 µm. (**c**) Quantification of intracellular fluorescence intensity in arbitrary unit (a.u.) measured in cells presented in b during the two hours of migration. The color of each line corresponds to the color of the arrow in (**b**).

Cell membrane disruption and repair in MDA-MB-231 migrating on collagen I. In order to assess if release of MbVS was accompanied by cell membrane disruptions, MDA-MB-231 cells were loaded with Fluo-4-AM and kinetics study of cell migration on collagen I was performed by fluorescence microscopy. Fluo-4-AM is a dye with a fluorescence intensity that considerably varies depending on intracellular calcium concentration. Weakly fluorescent in intact cells, where the cytoplasmic concentration of calcium is in the µM range, Fluo-4-AM exhibits a strong fluorescence increase when the integrity of plasma membrane is compromised since the calcium concentration increases strongly (mM). Images acquired in phase-contrast microscopy just before and after kinetics study ensured that cells have migrated on collagen I fibrils (Fig. 3a). We observed important variation of Fluo-4-AM fluorescence in several cells during migration (Fig. 3b and Supplementary video 4). The strong increase of fluorescence intensity revealed the presence of rupture(s) in cell membrane (Fig. 3b,c t = 32 min or t = 85 min). The recovery to a basal fluorescence intensity after about 1–2 min indicated that cell membrane resealed and calcium homeostasis was restored at the minute range (Fig. 3b,c t = 34 min or t = 86 min), in line with the timescale required for membrane repair in cells damaged by laser ablation[13,16,20,30,61]. We have concluded that shearing forces between collagen I fibrils and cell membrane of migrating MDA-MB-231 induce membrane disruptions that reseal at the minute range.

MDA-MB-231 cells exhibit a highly efficient membrane repair machinery. In order to investigate the membrane repair ability of MDA-MB-231 cells, plasma membrane was damaged by laser ablation and membrane repair was assayed by monitoring the kinetics of cell entry of membrane-impermeable FM1-43 dye, using a standard protocol[13,56]. Membrane resealing leads to a stop in the entry of FM1–43 molecules into the cytosol and therefore to a stop in the increase of the intracellular fluorescence intensity, whereas the absence of membrane resealing leads to a continuous entry of FM1-43 into the cytosol and a continuous and strong increase in the fluorescence intensity. Irradiation conditions were adjusted (110 mW) to cause mild membrane injury to cells, characterized by the entry of FM1-43 into the cytosol as early as a few seconds after laser ablation without the presence of a macroscopic tear at the site of membrane irradiation (Fig. 4a,b, frames 2, arrow). Two typical responses were observed within the 120 s following the membrane damage. 50% of cells exhibited an

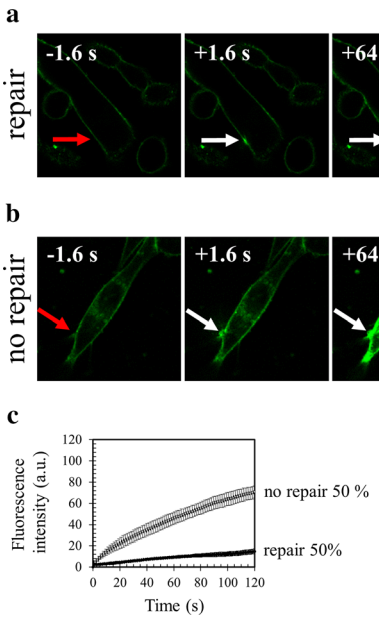

Figure 4. Responses of MDA-MB-231 cells to a membrane damage by laser ablation. Sequence of representative images showing the response of a MDA-MB-231 cell resealing (**a**) or not (**b**) a membrane damage performed by 110-mW infrared laser irradiation, in the presence of FM1-43 (green). Before irradiation, cells were washed 3 times in cold D-PBS containing 2 mM Ca^{2+} and then maintained in this medium. In all figures, the area of membrane irradiation is marked with a red arrow before irradiation and a white arrow after irradiation. Image frames 1 and 2 were recorded 1.6 s before and 1.6 s after irradiation, respectively; Image frames 3–4 were recorded 64 s and 120 s after irradiation, respectively, as indicated. Scale bar: 20 µm. (**c**) Kinetic data represent the FM1 – 43 fluorescence intensity integrated over whole cell sections, averaged for about 60 cells (+/ – SD) from five independent experiments (see also Supplementary table 1). For 50% of MDA-MB-231 cells, the fluorescence intensity reached a plateau after about 80 s (black filled circles). For the other half, a continuous and large increase of the fluorescence intensity was observed (empty circles), indicating the absence of membrane resealing.

increase of the fluorescence intensity limited to an area closed to the site of membrane injury (Fig. 4a and Supplementary video 5a). For these cells, we observed that the fluorescence intensity increased for about 80 s before reaching a plateau (Fig. 4c, black filled circles). The presence of the plateau indicated that the entry of FM1-43 was stopped and therefore that cell membrane resealed. The second half of cells presented a massive entry of FM1-43 (Fig. 4b and Supplementary video 5b) leading to a continuous and huge increase of the fluorescence intensity (Fig. 4c, empty circles), which indicated the absence of membrane resealing. This significant heterogeneity in the response of MDA-MB-231 cells to laser ablation has never been observed in our previous studies performed with perivascular, placental and muscle cells[13,20,30]. It suggests a phenotypic variability within the cell population. For the "repairing" MDA-MB-231 subpopulation, kinetics of FM1-43 entry into damaged cells and variations of the intracellular fluorescence intensity within the 120 s following membrane damage are in line with those observed in human myotubes[20] and syncytiotrophoblasts[30]. We have therefore concluded that MDA-MB-231 cells possess a cell machinery ensuring efficient repair of membrane damage, while this machinery is not systematically operational.

Anx are significantly expressed in MDA-MB-231 cells. Several members of the Anx family are instrumental for membrane repair in many cell types, namely AnxA1[12,14,62], AnxA2[16,48,62], AnxA4[15], AnxA5[13,20,30] and AnxA6[15,62]. In order to assess the relative expression of Anx in MDA-MB-231 cells, we prepared protein extracts from MDA-MB-231 and BeWo cells and analyzed the amount of Anx by western-blot (Fig. 5a,b and Supplementary Fig. 2). The choriocarcinoma BeWo cell line is placental in origin and the placenta is expected to be the richest organ in Anx in Humans (www.proteinatlas.org). BeWo cells served therefore as a positive control of the expression of Anx. In order to standardize measurements, MDA-MB-231 and BeWo protein extracts were analyzed on the same PVDF membrane and the band intensity relative to the Anx was reported to GAPDH, used as loading control. As an example, a typical result obtained for the detection of AnxA5 is presented in Fig. 5b. We observed that AnxA4 is hardly, if at all, detected in both cell lines. A significant expression of AnxA1, A2, A5, and A6 is observed. For these Anx, the expression level is systematically as high for MDA-MB-231 as for BeWo cells. We even observed that the expression of AnxA2 is stronger in MDA-MB-231 compared to BeWo cells. We can therefore conclude that four Anx (A1, A2, A5 and A6), which are known to participate in membrane repair, are highly expressed in MDA-MB-231 cells.

We then investigated the subcellular distribution of endogenous Anx in MDA-MB-231 cells. Immunocytofluorescence experiments confirmed that AnxA1, AxnA2, AnxA5 and AnxA6 are significantly expressed in

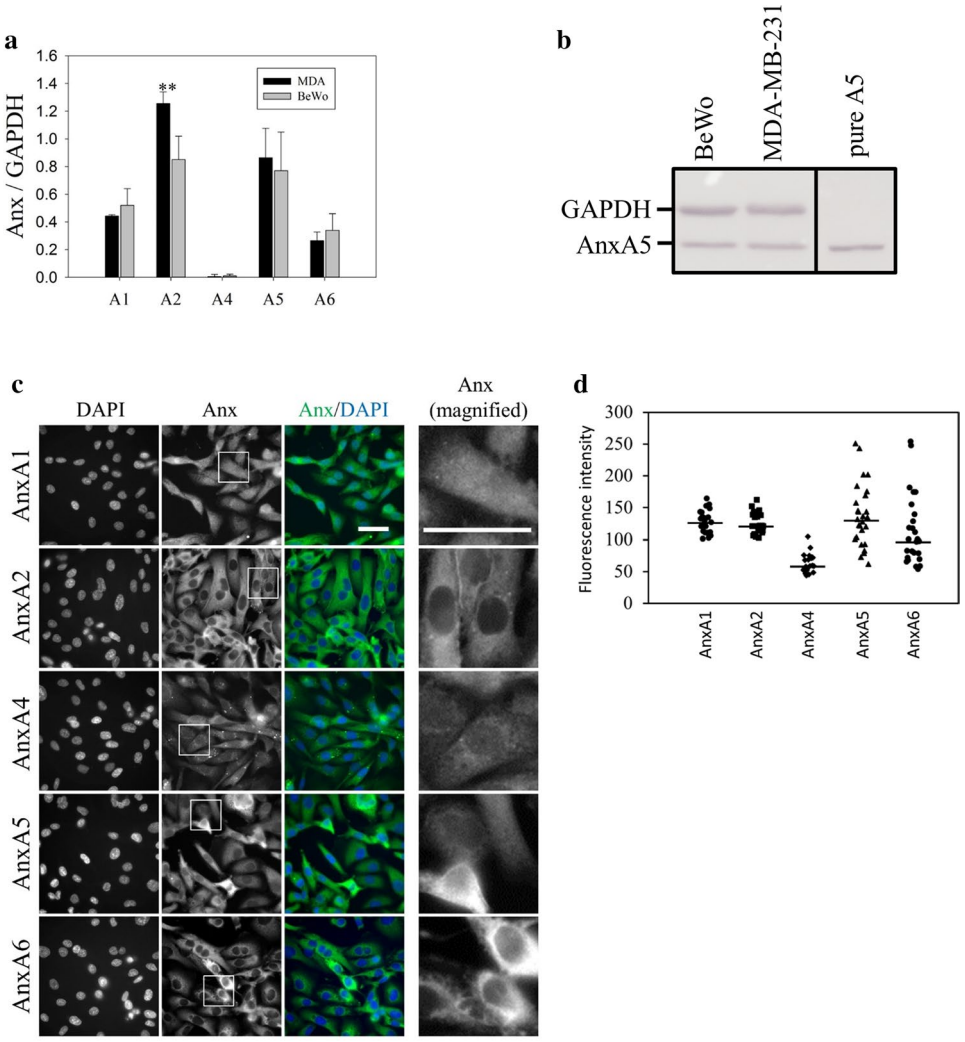

Figure 5. Expression and subcellular localization of endogenous Anx in MDA-MB-231. (**a**) 10 µg of protein extracts from MDA-MB-231 and BeWo cells were analyzed by western-blot. The gel analysis plugin of ImageJ was used to quantify the density of bands. The histogram presents mean values (± SD) of the ratio Anx/GAPDH from ten independent experiments. Student t Test for independent samples. $^{**}p < 0.01$. (**b**) Revelation of AnxA5 in MDA-MB-231 and BeWo cells compared to 50 ng purified recombinant AnxA5 (Pure A5), presented as an example. The whole membrane, together with representative western-blot analysis for AnxA1, A2, A4 and A6, are presented in Supplementary Fig. 2. (**c**) MDA-MB-231 cells were immunostained for AnxA1, AnxA2, AnxA4, AnxA5 and AnxA6 (green), as indicated, and counterstained with DAPI (blue). The right-hand column presents magnified images extracted from the "Anx" column (indicated by inserts). Scale bar: 40 µm. (**d**) Quantification of fluorescence intensities after immunostaining of endogenous Anx in MDA-MB-231 cells. Fluorescence intensities were measured from 8-bit images by drawing a circular ROI inside the cytoplasm and measuring the mean pixel value. Mean pixel values from at least 20 cells are presented. Horizontal bars represent median values. The variance value is 323, 268, 224, 2372 and 2909 for AnxA1, A2, A4, A5 and A6, respectively. The coefficient of variation is 14%, 13%, 24%, 35% and 47% for AnxA1, A2, A4, A5 and A6, respectively. The expression level of AnxA5 or AnxA6 is heterogenous from one MDA-MB-231 cell to another. In some cells, AnxA5 and AnxA6 are expressed at a very low level.

MDA-MB-231 cells whereas AnxA4 is weakly expressed (Fig. 5c). As observed in human myoblasts (our personal data) and murine neuroblasts[63], AnxA1 localizes in the nucleus and in the cytoplasm of MDA-MB-231 cells. Instead AnxA2, AnxA5 and AnxA6 are exclusively cytoplasmic. These results are consistent with previous studies for AnxA2[63] and AnxA6[64] but different for AnxA5[30,63], which has been reported to be present in nucleus and cytoplasm. The homogenous distribution of Anx within the cytoplasm supposes that it localizes in the cytosol. Strikingly, we observed that the expression level of AnxA5 or AnxA6 varies considerably from one MDA-MB-231 cell to another (Lower panels of Fig. 5c,d), whereas that of AnxA1 or AnxA2 is relatively constant (Higher panels of Fig. 5c,d). We observed that a cell expressing AnxA5 at a high level expresses also strongly AnxA6 (Supplementary Fig. 3). In addition, a low level of AnxA5 is systematically accompanied by a weak expression of AnxA6. This strong heterogeneity in the expression of AnxA5 and AnxA6 in MDA-MB-231 cells

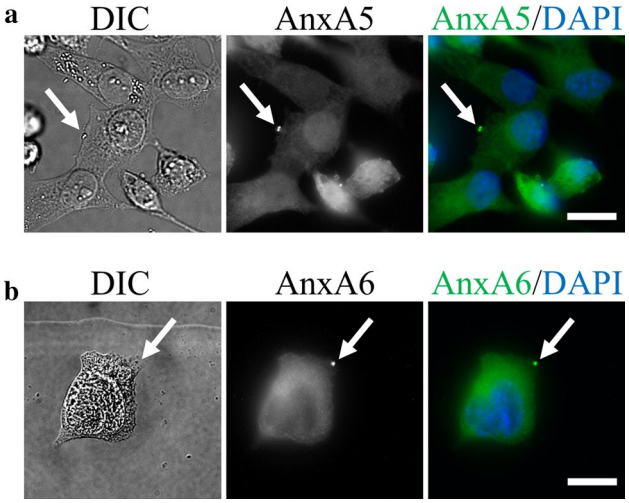

Figure 6. Subcellular localization of endogenous AnxA5 and AnxA6 in damaged MDA-MB-231. MDA-MB-231 cells were irradiated with a 110-mW infrared laser (white arrow) in DPBS + Ca^{2+}, then fixed and immunostained for AnxA5 (**a**) or AnxA6 (**b**). After laser injury, MDA-MB-231 cells exhibited an accumulation of AnxA5 or AnxA6 at the disruption site. Scale bar: 20 µm.

and the fact that some of them express at a low level both Anx are in line with the absence of membrane repair observed in a part of these cells damaged by laser ablation. This result suggests that AnxA5 and/or AnxA6 may participate in the membrane repair machinery of the MDA-MB-231 cells. Hereafter we have therefore focused our attention on AnxA5 and AnxA6.

AnxA5 and AnxA6 belong to the membrane repair machinery of MDA-MB-231 cells. Most, if not all, proteins that are involved in the repair machinery, i.e. dysferlin[8], AnxA1, AnxA2, AnxA6[12,14,65], AnxA5[13,30] and MG-53[17] are recruited to the membrane disruption site immediately after membrane injury. In order to assess whether AnxA5 and AnxA6 may be involved in the membrane repair machinery of MDA-MB-231 cells, we investigated the subcellular localization of both Anx after laser ablation. For this purpose, MDA-MB-231 cells were cultured on gridded coverslips, thus enabling accurate tracking of irradiated cells. After laser irradiation, cells were fixed, permeabilized and immunostained for AnxA5 (Fig. 6a) or AnxA6 (Fig. 6b). After laser injury, endogenous AnxA5 and AnxA6 were found specifically accumulated at the disruption site of MDA-MB-231 cells. We have previously shown that AnxA5 promotes membrane repair mainly by interacting with the edges of the torn membrane, where it forms bi-dimensional arrays that strengthen the membrane and prevent the expansion of the tear[13,20]. In addition, it has been proposed that AnxA6 is recruited to the wound edges, where it induces a constriction force enabling wound closure[15]. Interaction between Anx and damaged plasma membrane requires only the presence of phosphatidylserine in the membrane and Ca^{2+} at mM concentration. Therefore, it is likely that the recruitment of AnxA5 and AnxA6 at the disruption site is responsible for membrane resealing in MDA-MB-231 cells.

In order to confirm that AnxA5 and AnxA6 are required for membrane repair, both Anx were knocked-down in MDA-MB-231 cells using shRNA strategy. We estimated that the decrease of the expression of AnxA5 or AnxA6 in transduced cells was about 90% (Supplementary Fig. 4). AnxA5-deficient or AnxA6-deficient MDA-MB-231 cells were then submitted to membrane repair assay. After laser injury, we observed that AnxA5-deficient MDA-MB-231 cells exhibited a rapid and strong increase in the intracellular fluorescence intensity due to the entry of FM1-43 dye, indicating a major defect of membrane repair (Fig. 7a,c, middle panel). AnxA6-deficient MDA-MB-231 cells also exhibited a continuous entry of FM1-43 dye into the cytosol after membrane damage but in a lesser extent compared to AnxA5-deficient cells (Fig. 7b,c, right panel). The absence of plateau within 120 s after membrane damage indicates that these cells also present a defect of membrane repair. 120 s after membrane injury, imaging of FM1-43 by video-microscopy was stopped and gain and offset values were adjusted to obtain an unsaturated fluorescence image (Fig. 7d). We observed that most AnxA5-deficient MDA-MB-231 cells (n = 45 /49) exhibited a large membrane disruption at the wound site (Fig. 7d, left panel). We have proposed previously that AnxA5 molecules form 2D-arrays at the edges of the membrane disruption site in order to strengthen the membrane and to avoid the extension of the rupture[13,20,30], which has been recently confirmed on model membrane[66]. The hole present at the irradiation site suggests that plasma membrane has been torn. Lipid material, which is marked by the lipophilic dye FM1-43, is accumulated near the disruption site but looks insufficiently dense for plugging it. Strikingly, in the case of AnxA6-deficient MDA-MB-231 cells, we often (n = 36/51) observed that lipid material is concentrated far away from the membrane injury (Fig. 7d, right panel). If the repair mechanism relies on the formation of a lipid "patch" that is supposed to clog the membrane disruption, AnxA6-deficient cells would suffer from a defect in the recruitment of this lipid "patch". Altogether, these results led to conclude that AnxA5 and AnxA6 are instrumental for membrane repair in MDA-MB-231 cells.

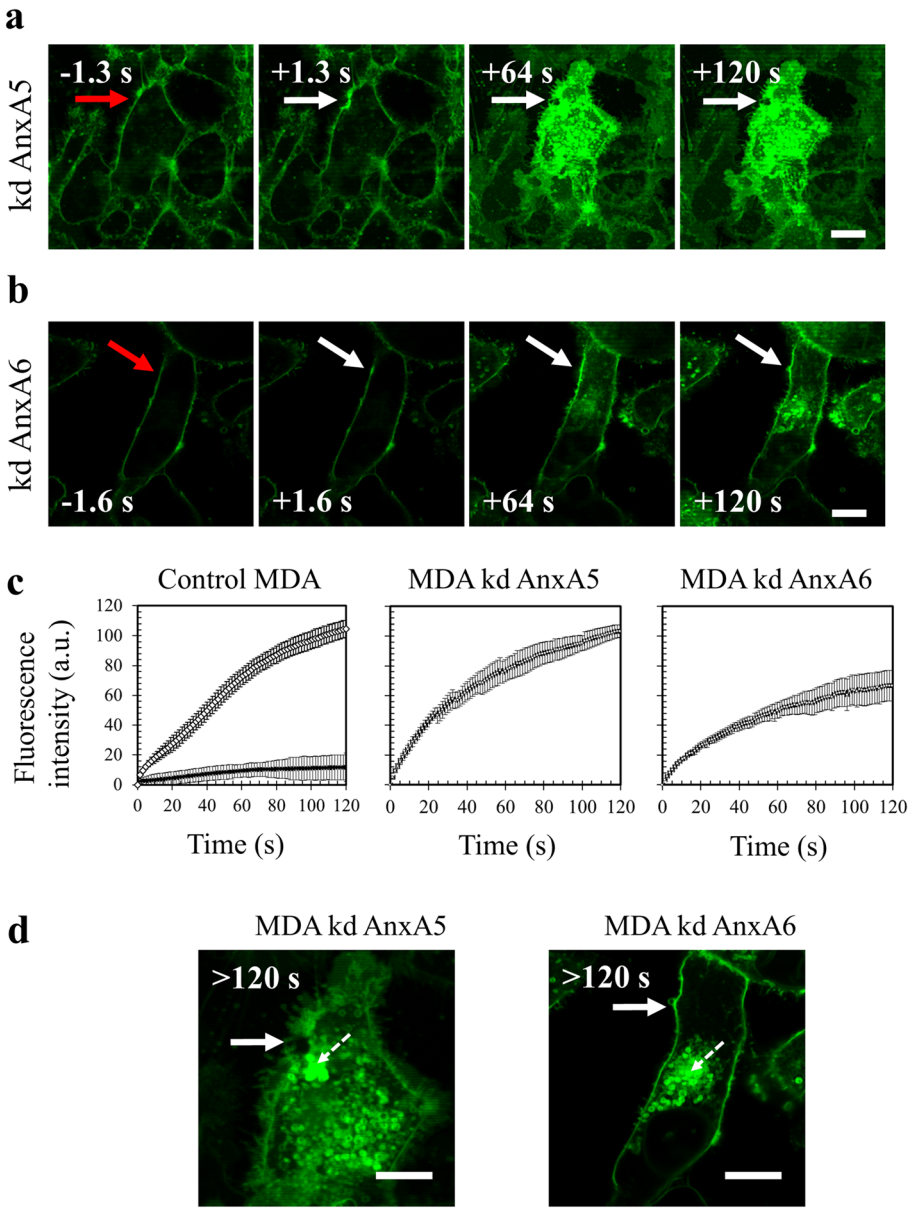

Figure 7. Responses of AnxA5-deficient or AnxA6-deficient MDA-MB-231 cells to a membrane damage by laser ablation. Sequence of representative images showing the response of an AnxA5-deficient (**a**) or an AnxA6-deficient MDA-MB-231 (**b**) cell after membrane damage performed by laser irradiation in the presence of FM1-43 (green) is presented. Cells were treated and presented as described in the legend of Fig. 4. Scale bar: 10 µm. (**c**) Kinetic data represent the FM1–43 fluorescence intensity integrated over whole cell sections, averaged for about 60 cells (±SD) from five independent experiments (see also Supplementary table 2). The response of control (control MDA), AnxA5-deficient (MDA kd AnxA5) and AnxA6-deficient (MDA kd AnxA6) MDA-MB-231 cells are presented. Control cells were MDA-MB-231 cells transduced with SCshRNA-containing lentiviral particles. For MDA kd AnxA5 and MDA kd AnxA6 a continuous and large increase of the fluorescence intensity was observed, indicating the absence of membrane resealing. (**d**) Zoomed and unsaturated images of kd AnxA5 and kd AnxA6 cells presented in a and b 120 s after membrane injury, respectively. Large filled and small dashed white arrows point out the wound site and the lipid material accumulating inside the cell after membrane injury, respectively. Scale bar: 10 µm.

AnxA5-AnxA6 deficient MDA-MB-231 cells suffer from a severe defect of membrane repair and die during migration on collagen I. Finally, we investigated the influence of knock-down in AnxA5 and/or AnxA6 on the migration of MDA-MB-231 cells on collagen I. For this purpose, we established a double knock-down AnxA5 and AnxA6 MDA-MB-231 cell line (hereafter named AnxA5-AnxA6 deficient MDA-MB-231 cells). MDA-MB-231 cells transduced together with AnxA5- and AnxA6- targeting shRNAs exhibited a decrease by about 73% and 99% for AnxA5 and AnxA6, respectively (Supplementary Fig. 5). As expected, AnxA5-AnxA6 deficient MDA-MB-231 cells suffer from a defect of membrane repair after laser damage (Sup-

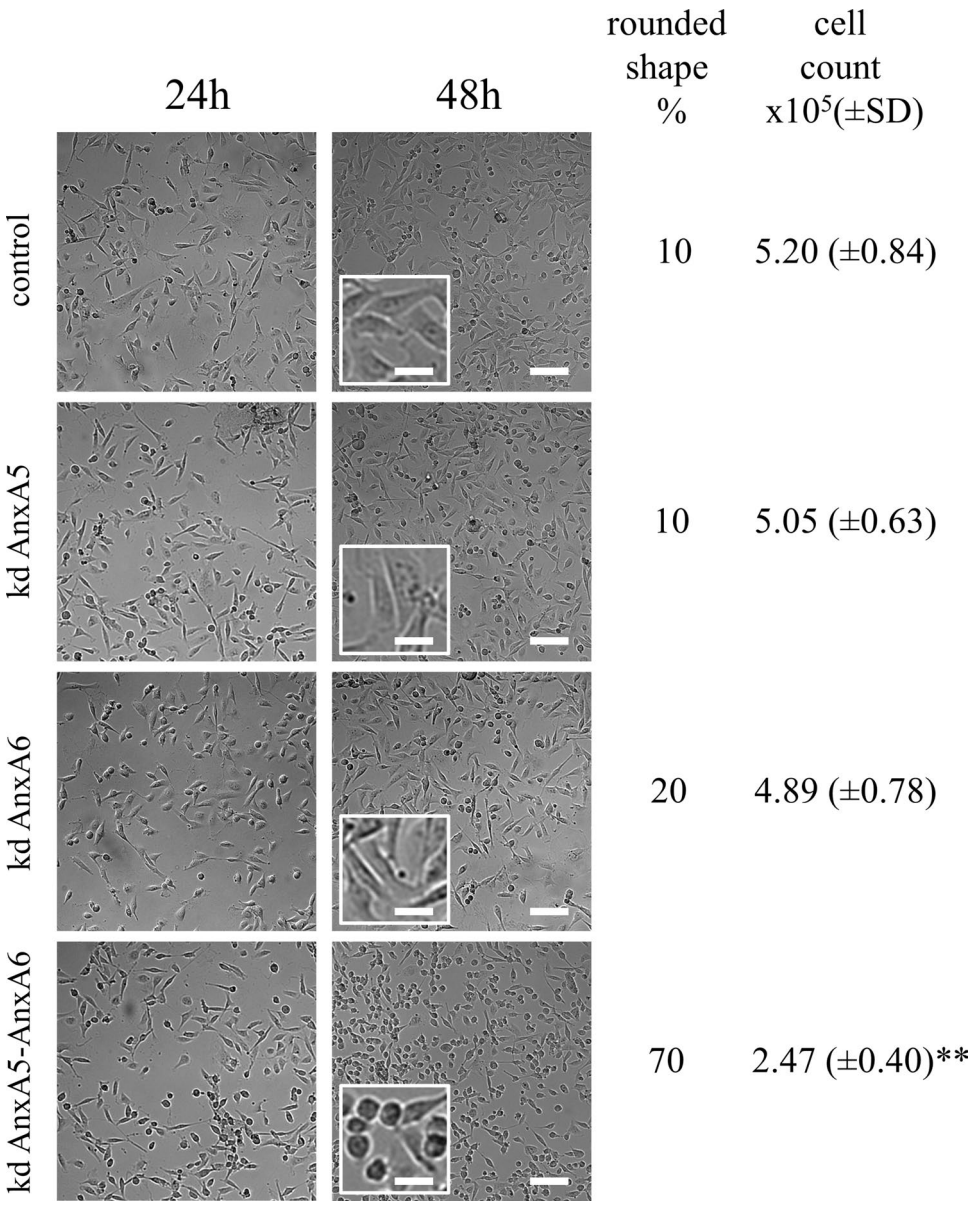

Figure 8. Responses of Anx-deficient MDA-MB-231 cells to membrane damages induced by migration on collagen I. $2{\cdot}10^5$ control, AnxA5-deficient, AnxA6-deficient or AnxA5-AnxA6 deficient MDA-MB-231 cells were seeded on a glass coverslip coated with collagen I. Control cells were MDA-MB-231 cells transduced with SCshRNA-containing lentiviral particles. 24 h (left panels) and 48 h (middle panels) after seeding, cells were imaged by phase contrast microscopy. At 48 h, the insert displays a magnified area from the image for the sake of clarity. At 48 h-post seeding, the percentage of cells displaying rounded shape was estimated using the ImageJ software. Rounded cells were defined as presenting a circularity ≥ 0.50, with circularity = 4*pi*(area/perimeter^2). Cells were then washed, trypsinized and counted. Mean values (±SD) from three independent experiments performed in triplicate are presented in the right lane. Student t Test for independent samples. $^{**}p < 0.01$. Scale bars: images, 100 µm; inserts, 25 µm.

plementary Fig. 6a,b). As observed for AnxA6-deficient MDA-MB-231 cells, lipid material appeared frequently concentrated far away from the membrane injury (Supplementary Fig. 6c).

In order to assess the influence of a defect of the membrane repair machinery in cell life during migration, we seeded $2{\cdot}10^5$ control or Anx-deficient MDA-MB-231 cells on a dish coated with collagen I and cells were imaged and counted 24 h and 48 h after seeding. We hypothesized that migration of Anx-deficient MDA-MB-231 on collagen I may lead to the death of cells and their detachment from the coverslip, due to un-resealed membrane damages. 24 h after seeding, we observed that Anx-deficient cells exhibit a cell density and morphology similar to control cells indicating that the deficiency in Anx does not disturb cell adhesion on collagen I-coated coverslip (Fig. 8, 24 h). 48 h after seeding, phase contrast microscopy imaging showed that cell density was

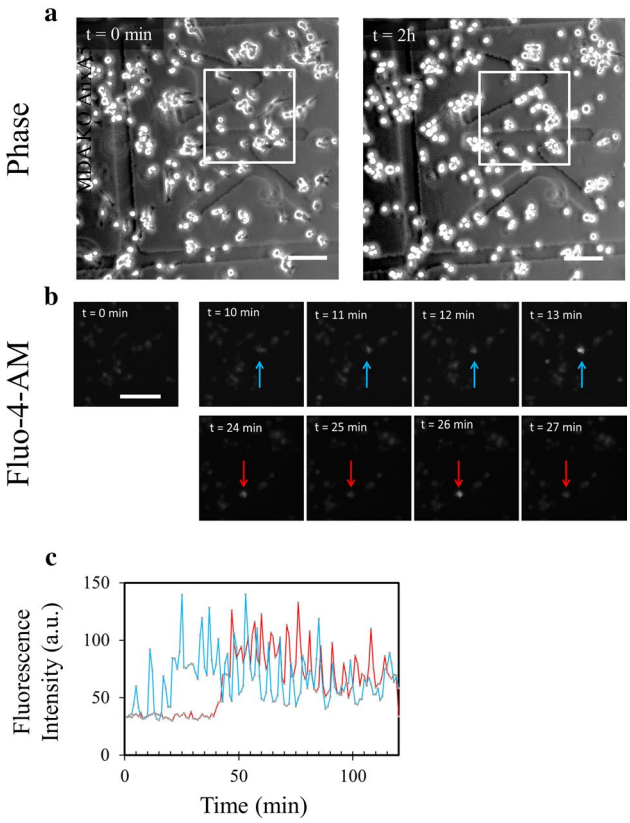

Figure 9. Highlighting un-resealed membrane damages in migrating AnxA5-AnxA6 deficient MDA-MB-231 cells. AnxA5-AnxA6 deficient MDA-MB-231 cells were treated as described in the legend of Fig. 3. (**a**) Images in phase-contrast microscopy were acquired before and after the kinetics study performed by fluorescence microscopy. (**b**) Fluorescence intensity variations of intracellular Fluo-4-AM studied in the course of time. Each colored arrow points out a cell of interest exhibiting a strong variation of the fluorescence intensity. Strong increases of fluorescence intensity are particularly observed at t = 11 min and t = 13 min (blue arrow) and t = 24 min and t = 26 min (red arrow). A decrease of fluorescence intensity is observed at t = 10 min and t = 12 min (blue arrow) and t = 25 min and t = 27 min (red arrow). Scale bar: 100 µm. (**c**) Quantification of intracellular fluorescence intensity in arbitrary unit (a.u.) measured in cells presented in b during the two hours of migration. The color of each line corresponds to the color of the arrow in (**b**).

similar between control and AnxA5-AnxA6 deficient cells, though the percentage of rounded cells was strongly increased (Fig. 8, 48 h).

Through video-microscopy analysis, we observed that elongated AnxA5-AnxA6 deficient MDA-MB-231 cells became rounded as soon as they were starting to migrate (Supplementary video 6). It was likely that rounded cells were dying cells, which were intended to be eliminated during washes prior to trypsinization. This was confirmed by cell counting, which showed that living adherent AnxA5-AnxA6 deficient cells represented in about half of the amount of control cells (Fig. 8). As control, we have analyzed the behavior of AnxA5-AnxA6 MDA seeded on gelatin, which corresponds to denaturated collagen I (Supplementary video 7). These cells migrated weakly and exhibited a number of rounded and living adherent cells similar to control cells. We observed that AnxA5 or AnxA6 deficiency had little effect on cell density and morphology, even the percentage of rounded cells appeared to be doubled for AnxA6-deficient MDA-MB-231 cells, without significant effect on the number of cells 48 h after seeding. A combined deficiency in AnxA5 and AnxA6 seems therefore to affect the migration of MDA-MB-231 cells on fibrillar collagen I.

To address the possibility that these AnxA5-AnxA6 deficient MDA-MB-231 cells suffer from a defect of membrane repair during their migration on collagen I, cells were loaded with Fluo-4-AM and kinetics study of cell migration on collagen I was performed by fluorescence microscopy. Images acquired in phase-contrast microscopy just before and after kinetics study ensured that cells have migrated (Fig. 9a). We observed important variation of Fluo-4-AM fluorescence in several cells during migration (Fig. 9b). The strong increase of fluorescence intensity revealed the presence of rupture(s) in cell membrane as observed in control cells (Fig. 3). However, in the case of AnxA5-AnxA6 deficient MDA-MB-231 cells we observed that over a large period the fluorescence oscillated between a high intensity and a lesser one (Fig. 9b,c). Through fluorescence video-microscopy, variations of intensity appeared as a flashing light (Supplementary video 8). It is unlikely that these variations were due to a series of damage and repair events. It is instead more relevant to think that it results from a strong increase of the intracellular calcium concentration subsequent to a membrane damage and an attempt

from the cell to counteract this Ca^{2+} excess, through Ca^{2+} absorption by mitochondria for example. Altogether these results suggest that AnxA5-AnxA6 deficient MDA-MB-231 cells are unable to reseal plasma membrane damages induced by their migration on collagen I.

Discussion

Migration on collagen I fibrils as a method for studying membrane repair. For reaching distant tissues, cancer cells are submitted to physical stresses during metastasis, due to their migration and invasion processes through dense extracellular matrix and due to intravasion and extravasion mechanisms for the entry into and the exit from the blood circulation, respectively. Shear stress induced by these processes may lead to cell membrane disruptions. This study aimed mainly at determining whether silencing of membrane repair machinery impairs survival of cancer cells during migration on extracellular matrix. It required first to find a method enabling to modelize shearing forces induced by the extracellular matrix. In this report, we have provided evidences that cell migration on collagen I fibrils leads to plasma membrane damages along with the release of membrane fragments in the wake of the cell. Membrane damage and release can be easily followed by fluorescence microscopy using labeled Ca^{2+} indicator and plasma membrane stain. Beyond of its interest for research in cancer biology, this method is an outstanding tool for studying membrane repair in cells that exhibit the capacity of migration, notably epithelial and endothelial cells. It could replace current artificial methods such as laser irradiation, permeabilization using detergent, sprinkling with glass beads or scratching with a needle, that are far away from physiological injuries.

AnxA5 and A6 belong to the membrane repair machinery of MDA-MB-231 cells. We then needed to identify proteins belonging to the membrane repair machinery. Several Anx have been shown to participate in membrane repair processes in different cell types[6,67], and particularly in cancer cells[15,48,49]. They constituted therefore prime targets for this achievement. Even though AnxA4 has been shown to play an instrumental role in membrane repair of MCF-7 cells[15], we observed that it is weakly expressed in MDA-MB-231 cells, suggesting its participation in membrane resealing is unlikely. However, AnxA1, A2, A5 and A6 are highly expressed in MDA-MB-231 cells and could be expected to participate in membrane resealing. Our attention focused particularly on AnxA5 and AnxA6, which exhibit varying intracellular concentrations. This heterogeneity of Anx expression probably explains discrepancy in the ability of MDA-MB-231 cells to reseal damaged plasma membrane. Our results demonstrate that AnxA5 and AnxA6 are instrumental for membrane repair in MDA-MB-231 cells. Whether the description of mechanisms related to membrane resealing in cancer cells was outside the scope of this study, some observations that we have done gave interesting clues on the role played by AnxA5 and AnxA6. We have previously proposed that AnxA5 forms 2D-arrays at the edges of the torn membrane allowing to strengthen the membrane and prevent the expansion of the tear[13,20,30]. This hypothesis has been recently confirmed by a sophisticated study performed by Scheuring and collaborators, using notably high-speed atomic force microscopy[66]. They showed that AnxA5 self-assembly into lattices decreases lipid diffusivity, increases membrane thickness and increases lipid order. All together these results show that the formation of AnxA5 2D-arrays at the edges of the torn membrane induces a transition phase that stabilizes and structures the membrane into a gel phase. Here, we have shown that endogenous AnxA5 is recruited rapidly at the disruption site in MDA-MB-231 cells, where it probably self-assembles upon binding to the damaged membrane and promote membrane repair. Damage by laser irradiation in AnxA5-deficient MDA-MB-231 cells leads to the absence of membrane repair, which seems to be due to the expansion of the breach becoming too large to be plugged by the lipid "patch". This observation is totally in line with the expected function of AnxA5 in membrane repair that we have previously reported.

AnxA6 is an unusual family member with two instead of one Anx core domains, each domain being composed by four 70-amino acid repeats. Together with other Anx, AnxA6 has been shown to assemble at the site of cell membrane damage and participate in membrane resealing in muscle[14,68,69] and cancer cells as well[15]. A specific role for AnxA6 in membrane resealing of damaged MCF-7 cells have been previously proposed[15]. From wound edges curved in out-of-plane by the action of AnxA4, AnxA6 induces constriction force responsible for the closure of the hole. It is important to note that MCF-7 cells were exposed to strong injuries by laser irradiation inducing a large wound diameter (up to 3 µm) in this study. As the membrane repair mechanism may vary depending on the cell type, the extent of the damage and the spatial position of the injury[6,15,70], it is likely that the role played by AnxA6 for resealing MDA-MB-231 cells is slightly different in our study. Here, we show that AnxA6-deficient MDA-MB-231 cells suffer from a defect of membrane repair, which seems to be linked to the absence of the recruitment of cytoplasmic lipid material, ie the lipid "patch", to the site of membrane damage. The presence of two Anx core domains gives the ability to AnxA6 to bridge two adjacent membranes, such as plasma membrane and cytoplasmic lipid vesicle. In addition, phylogenetic analysis of Anx has shown that the N-terminal core domain of AnxA6 is similar to AnxA3 whereas the C-terminal one is similar to AnxA5[71]. It has been shown that Anx induce different and specific membrane morphologies upon interaction[72]. For instance, AnxA3 rolls the membrane in a fragmented manner from free edges, producing multiple thin rolls, whereas AnxA5 induces cooperative roll-up of the membrane. AnxA6 may therefore induce multiple membrane rearrangements at the disruption site at the interface between free edges of the damaged plasma membrane and the intracellular lipid "patch". We hypothesize that the absence of AnxA6 may be responsible for the lack of recruitment of the lipid "patch".

Defective membrane repair machinery impairs survival of invasive cancer cells. The migration of MDA-MB-231 cells on fibrillar collagen I is accompanied by the release of membrane fragments responsible for the disruption of the cell membrane. In wild-type cells, in the presence of AnxA5 and AnxA6, these

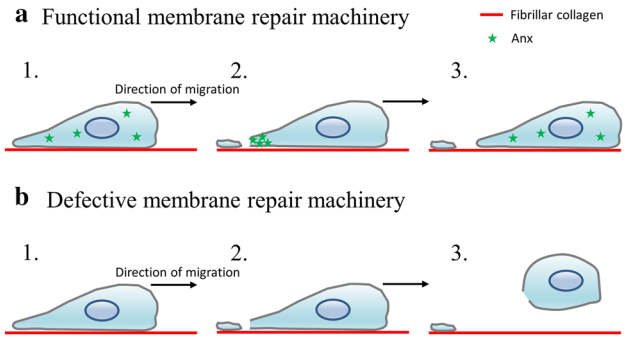

Figure 10. Model of migration of MDA-MB-231 cells equipped with a functional or defective membrane repair machinery. (**a**) In wild-type cells, migration on fibrillar collagen I induces the release of membrane fragments responsible for membrane injuries (Step 1). Anx, notably AnxA5 and AnxA6, are recruited to the disruption site, where they promote membrane repair (Step 2). Once the cell is repaired, Anx return to the cytosol (Step 3). (**b**) In cells presenting defective membrane repair, due for example to the absence of Anx, membrane injuries created by the migration on collagen I fibrils are not resealed (Step 2). This leads to the death of cells, which are released from the substrate (Step 3).

membrane injuries are resealed in less than a minute (Fig. 10a). As observed for damage by laser irradiation, it is likely that the increase of intracellular Ca^{2+} concentration induces the recruitment of Anx at the disruption site, where they promote membrane resealing. Once membrane repair is done, Anx come back to the cytosol and the cell can continue to migrate. The combined inhibition of the expression of AnxA5 and AnxA6 leads to a major defect of the membrane repair machinery. In MDA-MB-231 cells, this silencing leads to the incapacity of cells to migrate on fibrillar collagen I (Fig. 10b). In this case, disruptions due to migration are indeed not repaired leading to cell death. Consequently, cell migration is finally discontinued. Strikingly, we have observed that the inhibition of only AnxA5 or AnxA6 was not sufficient to induce death of cells and the stop of migration. It is likely that shear stress induced by collagen fibrils on cell membrane was minor force leading to small ruptures (few hundreds nm), smaller than those created by laser irradiation (1 µm). In this case, the low residual concentration of AnxA5 or AnxA6 may be sufficient for the achievement of membrane repair. One can also envision that the lack of AnxA5 or AnxA6 may be compensated by other Anx. In a physiological context, we hypothesize that mechanical stress would be stronger than in our in vitro experimental conditions. Indeed, a cell that migrates in vivo through the extracellular matrix is submitted to shear forces on the whole surface of the plasma membrane, whereas in our in vitro experimental model shear forces affect only plasma membrane at the interface interacting with the substrate. In addition, we can expect that shear forces induced by other cells during intravasion and extravasion processes are likely to be forces with greater strength.

In conclusion, we show here that silencing of the membrane repair machinery induces a stop of migration of cancer cells and constitutes a promising approach for inhibiting cancer metastasis.

Received: 15 July 2020; Accepted: 17 November 2020
Published online: 11 December 2020

References

1. McNeil, P. L. & Ito, S. Gastrointestinal cell plasma membrane wounding and resealing in vivo. *Gastroenterology* **96**, 1238–1248 (1989).
2. McNeil, P. L. & Ito, S. Molecular traffic through plasma membrane disruptions of cells in vivo. *J. Cell Sci.* **96**(Pt 3), 549–556 (1990).
3. McNeil, P. L. & Khakee, R. Disruptions of muscle fiber plasma membranes. Role in exercise-induced damage. *Am. J. Pathol.* **140**, 1097–1109 (1992).
4. Clarke, M. S., Caldwell, R. W., Chiao, H., Miyake, K. & McNeil, P. L. Contraction-induced cell wounding and release of fibroblast growth factor in heart. *Circ. Res.* **76**, 927–934 (1995).
5. McNeil, & Steinhardt, R. A. Plasma membrane disruption: Repair, prevention, adaptation. *Annu. Rev. Cell Dev. Biol.* **19**, 697–731 (2003).
6. Jimenez, A. J. & Perez, F. Plasma membrane repair: The adaptable cell life-insurance. *Curr. Opin. Cell Biol.* **47**, 99–107 (2017).
7. Griffin, D. A. *et al.* Defective membrane fusion and repair in *Anoctamin5* -deficient muscular dystrophy. *Hum. Mol. Genet.* **25**, 1900–1911 (2016).
8. Bansal, D. *et al.* Defective membrane repair in dysferlin-deficient muscular dystrophy. *Nature* **423**, 168–172 (2003).
9. Glover, L. & Brown, R. H. Dysferlin in membrane trafficking and patch repair. *Traffic* **8**, 785–794 (2007).
10. Huang, Y. *et al.* AHNAK, a novel component of the dysferlin protein complex, redistributes to the cytoplasm with dysferlin during skeletal muscle regeneration. *FASEB J.* **21**, 732–742 (2007).
11. Chrobáková, T. *et al.* Mutations in Czech LGMD2A patients revealed by analysis of calpain3 mRNA and their phenotypic outcome. *Neuromuscul. Disord.* **14**, 659–665 (2004).
12. Lennon, N. J. *et al.* Dysferlin interacts with annexins A1 and A2 and mediates sarcolemmal wound-healing. *J. Biol. Chem.* **278**, 50466–50473 (2003).
13. Bouter, A. *et al.* Annexin-A5 assembled into two-dimensional arrays promotes cell membrane repair. *Nat. Commun.* **2**, 270 (2011).
14. Roostalu, U. & Strähle, U. In vivo imaging of molecular interactions at damaged sarcolemma. *Dev. Cell* **22**, 515–529 (2012).

15. Boye, T. L. *et al.* Annexin A4 and A6 induce membrane curvature and constriction during cell membrane repair. *Nat. Commun.* **8**, 1623 (2017).
16. Koerdt, S. N. & Gerke, V. Annexin A2 is involved in Ca 2+-dependent plasma membrane repair in primary human endothelial cells. *Biochim. Biophys. Acta Mol. Cell Res.* **1864**, 1046–1053 (2017).
17. Cai, C. *et al.* MG53 nucleates assembly of cell membrane repair machinery. *Nat. Cell Biol.* **11**, 56–64 (2009).
18. Terasaki, M., Miyake, K. & McNeil, P. L. Large plasma membrane disruptions are rapidly resealed by Ca2+-dependent vesicle-vesicle fusion events. *J. Cell Biol.* **139**, 63–74 (1997).
19. McNeil, P. L., Vogel, S. S., Miyake, K. & Terasaki, M. Patching plasma membrane disruptions with cytoplasmic membrane. *J. Cell Sci.* **113**, 1891–1902 (2000).
20. Carmeille, R. *et al.* Membrane repair of human skeletal muscle cells requires Annexin-A5. *Biochim. Biophys. Acta Mol. Cell Res.* **1863**, 2267–2279 (2016).
21. Moss, S. E. & Morgan, R. O. The annexins. *Genome Biol.* **5**, 219 (2004).
22. Gerke, V., Creutz, C. E. & Moss, S. E. Annexins: Linking Ca^{2+} signalling to membrane dynamics. *Nat. Rev. Mol. Cell Biol.* **6**, 449–461 (2005).
23. Andree, H. A. *et al.* Binding of vascular anticoagulant alpha (VAC alpha) to planar phospholipid bilayers. *J. Biol. Chem.* **265**, 4923–4928 (1990).
24. Blackwood, R. A. & Ernst, J. D. Characterization of Ca2(+)-dependent phospholipid binding, vesicle aggregation and membrane fusion by annexins. *Biochem. J.* **266**, 195–200 (1990).
25. Monastyrskaya, K., Babiychuk, E. B., Hostettler, A., Rescher, U. & Draeger, A. Annexins as intracellular calcium sensors. *Cell Calcium* **41**, 207–219 (2007).
26. Kaetzel, M. A. *et al.* Phosphorylation mutants elucidate the mechanism of annexin IV-mediated membrane aggregation. *Biochemistry* **40**, 4192–4199 (2001).
27. Lambert, O., Gerke, V., Bader, M. F., Porte, F. & Brisson, A. Structural analysis of junctions formed between lipid membranes and several annexins by cryo-electron microscopy. *J. Mol. Biol.* **272**, 42–55 (1997).
28. Oling, F., Bergsma-Schutter, W. & Brisson, A. Trimers, dimers of trimers, and trimers of trimers are common building blocks of annexin a5 two-dimensional crystals. *J. Struct. Biol.* **133**, 55–63 (2001).
29. Voges, D. *et al.* Three-dimensional structure of membrane-bound annexin V A correlative electron microscopy-X-ray crystallography study. *J. Mol. Biol.* **238**, 199–213 (1994).
30. Carmeille, R. *et al.* Annexin-A5 promotes membrane resealing in human trophoblasts. *Biochim. Biophys. Acta* **1853**, (2015).
31. Liu, J. *et al.* Dysferlin, a novel skeletal muscle gene, is mutated in Miyoshi myopathy and limb girdle muscular dystrophy. *Nat. Genet.* **20**, 31–36 (1998).
32. Minetti, C. *et al.* Mutations in the caveolin-3 gene cause autosomal dominant limb-girdle muscular dystrophy. *Nat. Genet.* **18**, 365–368 (1998).
33. Swaminathan, V. *et al.* Mechanical stiffness grades metastatic potential in patient tumor cells and in cancer cell lines. *Cancer Res.* **71**, 5075–5080 (2011).
34. Wirtz, D., Konstantopoulos, K. & Searson, P. C. The physics of cancer: The role of physical interactions and mechanical forces in metastasis. *Nat. Rev. Cancer* **11**, 512–522 (2011).
35. Chuthapisith, S. *et al.* Annexins in human breast cancer: Possible predictors of pathological response to neoadjuvant chemotherapy. *Eur. J. Cancer* **45**, 1274–1281 (2009).
36. Ma, R.-L., Shen, L.-Y. & Chen, K.-N. Coexpression of ANXA2, SOD2 and HOXA13 predicts poor prognosis of esophageal squamous cell carcinoma. *Oncol. Rep.* **31**, 2157–2164 (2014).
37. Yang, T. *et al.* Prognostic and diagnostic significance of annexin A2 in colorectal cancer. *Color. Dis.* **15**, e373–e381 (2013).
38. Yao, H. *et al.* Identification of metastasis associated proteins in human lung squamous carcinoma using two-dimensional difference gel electrophoresis and laser capture microdissection. *Lung Cancer* **65**, 41–48 (2009).
39. Zhang, Q. *et al.* Upregulated expression of Annexin II is a prognostic marker for patients with gastric cancer. *World J. Surg. Oncol.* **10**, 103 (2012).
40. Wei, B., Guo, C., Liu, S. & Sun, M.-Z. Annexin A4 and cancer. *Clin. Chim. Acta* **447**, 72–78 (2015).
41. Deng, S. *et al.* Annexin A1, A2, A4 and A5 play important roles in breast cancer, pancreatic cancer and laryngeal carcinoma, alone and/or synergistically. *Oncol. Lett.* **5**, 107–112 (2013).
42. Duncan, R., Carpenter, B., Main, L. C., Telfer, C. & Murray, G. I. Characterisation and protein expression profiling of annexins in colorectal cancer. *Br. J. Cancer* **98**, 426–433 (2008).
43. Wehder, L. *et al.* Annexin A5 is involved in migration and invasion of oral carcinoma. *Cell Cycle* **8**, 1552–1558 (2009).
44. Peng, B., Liu, S., Guo, C., Sun, X. & Sun, M.-Z. ANXA5 level is linked to *in vitro* and *in vivo* tumor malignancy and lymphatic metastasis of murine hepatocarcinoma cell. *Futur. Oncol.* **12**, 31–42 (2016).
45. Ding, X.-M. *et al.* Effects of silencing annexin A5 on proliferation and invasion of human cholangiocarcinoma cell line. *Eur. Rev. Med. Pharmacol. Sci.* **21**, 1477–1488 (2017).
46. Wu, B. *et al.* Up-regulation of Anxa2 gene promotes proliferation and invasion of breast cancer MCF-7 cells. *Cell Prolif.* **45**, 189–198 (2012).
47. Koumangoye, R. B. *et al.* Reduced annexin A6 expression promotes the degradation of activated epidermal growth factor receptor and sensitizes invasive breast cancer cells to EGFR-targeted tyrosine kinase inhibitors. *Mol. Cancer* **12**, 167 (2013).
48. Jaiswal, J. K. *et al.* S100A11 is required for efficient plasma membrane repair and survival of invasive cancer cells. *Nat. Commun.* **5**, 3795 (2014).
49. Sønder, S. L. *et al.* Annexin A7 is required for ESCRT III-mediated plasma membrane repair. *Sci. Rep.* **9**, 6726 (2019).
50. Thompson, E. W. *et al.* Association of increased basement membrane invasiveness with absence of estrogen receptor and expression of vimentin in human breast cancer cell lines. *J. Cell. Physiol.* **150**, 534–544 (1992).
51. Ramaswamy, S., Ross, K. N., Lander, E. S. & Golub, T. R. A molecular signature of metastasis in primary solid tumors. *Nat. Genet.* **33**, 49–54 (2003).
52. Gilkes, D. M. *et al.* Collagen Prolyl Hydroxylases Are Essential for Breast Cancer Metastasis. *Cancer Res.* **73**, 3285–3296 (2013).
53. Juin, A. *et al.* Physiological type I collagen organization induces the formation of a novel class of linear invadosomes. *Mol. Biol. Cell* **23**, 297–309 (2012).
54. Di Martino, J. *et al.* 2D and 3D Matrices to Study Linear Invadosome Formation and Activity. *J. Vis. Exp.* https://doi.org/10.3791/54911 (2017).
55. Meijering, E., Dzyubachyk, O. & Smal, I. Methods for cell and particle tracking. *Methods Enzymol.* **504**, 183–200 (2012).
56. Carmeille, R., Croissant, C., Bouvet, F. & Bouter, A. Membrane repair assay for human skeletal muscle cells. *Methods Mol. Biol.* **1668**, 195–207 (2017).
57. Juin, A. *et al.* Discoidin domain receptor 1 controls linear invadosome formation via a Cdc42–Tuba pathway. *J. Cell Biol.* **207**, 517–533 (2014).
58. Ezzoukhry, Z. *et al.* TGF-β1 promotes linear invadosome formation in hepatocellular carcinoma cells, through DDR1 up-regulation and collagen I cross-linking. *Eur. J. Cell Biol.* **95**, 503–512 (2016).
59. Ma, L. *et al.* Discovery of the migrasome, an organelle mediating release of cytoplasmic contents during cell migration. *Cell Res.* **25**, 24–38 (2015).

60. Wu, D. *et al.* Pairing of integrins with ECM proteins determines migrasome formation. *Cell Res.* **27**, 1397–1400 (2017).
61. McNeil, P. L. & Kirchhausen, T. An emergency response team for membrane repair. *Nat. Rev. Mol. Cell Biol.* **6**, 499–505 (2005).
62. Demonbreun, A. R. *et al.* An actin-dependent annexin complex mediates plasma membrane repair in muscle. *J. Cell Biol.* **213**, 705–718 (2016).
63. Skrahina, T., Piljić, A. & Schultz, C. Heterogeneity and timing of translocation and membrane-mediated assembly of different annexins. *Exp. Cell Res.* **314**, 1039–1047 (2008).
64. Vilá de Muga, S. *et al.* Annexin A6 inhibits Ras signalling in breast cancer cells. *Oncogene* **28**, 363–377 (2009).
65. McNeil, A. K., Rescher, U., Gerke, V. & McNeil, P. L. Requirement for annexin A1 in plasma membrane repair. *J. Biol. Chem.* **281**, 35202–35207 (2006).
66. Lin, Y. C., Chipot, C. & Scheuring, S. Annexin-V stabilizes membrane defects by inducing lipid phase transition. *Nat. Commun.* **11**, 230 (2020).
67. Draeger, A., Monastyrskaya, K. & Babiychuk, E. B. Plasma membrane repair and cellular damage control: The annexin survival kit. *Biochem. Pharmacol.* **81**, 703–712 (2011).
68. Swaggart, K. A. *et al.* Annexin A6 modifies muscular dystrophy by mediating sarcolemmal repair. *Proc. Natl. Acad. Sci. U. S. A.* **111**, 6004–6009 (2014).
69. Demonbreun, A. R. *et al.* Recombinant annexin A6 promotes membrane repair and protects against muscle injury. *J. Clin. Invest.* **129**, 4657–4670 (2019).
70. Boye, T. L. & Nylandsted, J. Annexins in plasma membrane repair. *Biol. Chem.* **397**, 961–969 (2016).
71. Morgan, R. O. & Fernández, M. P. Molecular phylogeny of annexins and identification of a primitive homologue in Giardia lamblia. *Mol. Biol. Evol.* **12**, 967–979 (1995).
72. Boye, T. L. *et al.* Annexins induce curvature on free-edge membranes displaying distinct morphologies. *Sci. Rep.* **8**, 10309 (2018).

Acknowledgements

This work was funded by the Cancéropole Grand-Sud-Ouest (grant 2015-E21 to A.B.) and Ligue Contre Le Cancer Gironde (grant 191796 to A.B.). The help of Marion Decossas, Elise Dargelos, Sylvie Poussard and Olivier Lambert is acknowledged for the use the Leica DMI6000B microscope. Christel Poujol and Sébastien Marais are acknowledged for the help in membrane repair assays that were done in the Bordeaux Imaging Center a service unit of the CNRS-INSERM and Bordeaux University, member of the national infrastructure France BioImaging supported by the French National Research Agency (ANR-10-INBS-04). The authors thank the staff of Vect'UB, the vectorology platforms (INSERM US 005 – CNRS UMS 3427- TBM-Core, Université de Bordeaux, France) for technical assistance. The authors declare no competing financial interests.

Author contributions

F. B. and A. B. performed the majority of experiments with assistance from M. R. (study of migrasome and set-up of protocol for kinetics study of cell migration), E. B. (study of migrasome), C. C. (analysis by western-blot of Anx-deficient cells), L. F. (analysis of survival of Anx5- or AnxA6-deficient cells). A. B. coordinated the entire project. A. B., V. M. and F. S. designed the experiments and contributed to the writing of the manuscript.

Funding

This work was funded by the Cancéropole Grand-Sud-Ouest (grant 2015-E21 to A.B.) and Ligue Contre Le Cancer Gironde (grant 191796 to A.B.).

Competing interests

The authors declare no competing interests.

Additional information

Supplementary information is available for this paper at https://doi.org/10.1038/s41598-020-77902-5.

Correspondence and requests for materials should be addressed to A.B.

Reprints and permissions information is available at www.nature.com/reprints.

Publisher's note Springer Nature remains neutral with regard to jurisdictional claims in published maps and institutional affiliations.